A Self-Organized Two-Dimensional Bimolecular Structure

L. Scudiero, K. W. Hipps,* and Dan E. Barlow

Department of Chemistry and Material Science Program, Washington State University, Pullman, Washington 99164-4630

Received: August 29, 2002; In Final Form: November 18, 2002

The production of a novel two-dimensional bimolecular surface structure using weak noncovalent interactions is demonstrated and observed by scanning tunneling microscopy (STM). This work follows closely the three-dimensional ideas of crystal engineering and applies the concepts of supramolecular synthons to molecular systems constrained to two dimensions by physisorption on a conducting surface. We demonstrate a well-ordered planar structure that self-assembles through the influence of fluorine−phenyl interactions. This study provides a concrete example of the systematic design of self-organized layers. Fully fluorinated cobalt phthalocyanine (F_{16}CoPc) thermally deposited onto gold is characterized by RAIRS, XPS, and STM. UPS spectra of thin films of CoPc, F16CoPc, and nickel tetraphenylporphyrin (NiTPP) on gold are reported and their relative surface charges are compared. STM images of single molecular layers of F_{16}CoPc, NiTPP, and mixtures of NiTPP with F_{16}CoPc and of NiTPP with CoPc are also presented. While NiTPP/F16CoPc spontaneously forms a well-ordered 1:1 structure, NiTPP/CoPc forms a two-dimensional solid solution.

Introduction

Noncovalent interactions are critical to an understanding of a wide range of disciplines from molecular biology to materials science.[1,2] In the materials field, noncovalent interactions are an essential feature in the rational design of solid-state structures (crystal engineering). Desiraju has coined the phrase "supramolecular synthons" which are intermolecular interactions that play the same focusing role in supramolecular synthesis that conventional synthons do in molecular synthesis.[3] If molecules are built by connecting atoms with covalent bonds, supramolecules are built by connecting molecules with intermolecular interactions. Directional intermolecular interactions can be combined by a designed placement of functional groups in the molecular skeleton to generate supramolecular structures. Crystal engineering is concerned with the systematic architecture of crystal structures, and the use of noncovalent interactions now forms a central component in this discipline. Among these noncovalent interactions, hydrogen bonding is the most common; however, other interactions including halogen−halogen,[4] halogen−nitrogen,[3,5,6] halogen−oxygen,[3] electrostatic interactions,[7−11] and weak electron donor−acceptor complexation[12] have been used to organize molecules within a crystal. Among the systems exhibiting electrostatic interactions, the most thoroughly studied both experimentally[7−11,13] and theoretically[10,14−16] are the fluorine-substituted aromatic−aromatic interactions, with perfluorophenyl−phenyl interactions playing a featured role.

Upon the basis of the analogy to the concept of supramolecular synthons in solid and fluid phase, we paraphrase and expand on Desiraju's statements about the solid state to apply to the adsorbed state: There is a particular relevance of the surface state to supramolecular synthesis with physisorbed molecules, because many of the weaker interactions used in generating synthons are probably distorted or destroyed in fluid solution and in chemisorption. The weak lateral forces exerted by the surface upon physisorbed molecules, and the image charges that occur in metal substrates, allow these weaker intermolecular forces to play a significant role in the formation of long-range order in the adsorbed phase.

While many of the supramolecular synthons developed for crystal synthesis will be inappropriate for generating surface structures because of the planar template effect of the substrate, others may have their stability enhanced by the reduction in entropy and by the steric constraints imposed by the surface. Judicious use of weakly chemisorbing moieties within a molecular building block could also aid in the design of supramolecular structures that were *not* planar by design. Once a desired monolayer structure is generated, it may become possible to design three-dimensional-layered structures on the basis of that initial template. Note that we have restricted our consideration to systems where the interaction with the substrate is weak and preferably physisorptive in nature. This is to ensure that the lateral intermolecular interactions can play a significant role in coadsorbate ordering.

The most thoroughly studied case of coadsorbate-induced ordering is CO + benzene adsorbed on Pt, Rh, and Pd.[17−20] At low coverage on all these metals, benzene does NOT order. With the addition of CO, however, well-ordered structures result. Mate and Somorjai were the first to postulate a vertical dipole−dipole interaction mechanism for the ordering process.[21] Adsorbates with a positive dipole moment relative to the surface form-ordered structures when coadsorbed with CO (having a negative moment), while segregation or disorder occurs when CO is coadsorbed with an adsorbate with a similarly oriented dipole moment.[22] The CO + benzene like systems, however, are not particularly appropriate models for the noncovalent interactions envisaged here because both species undergo significant bonding with the metal substrates studied. Benzene transfers charge from its π system to the Rh, Pt, or Pd surface, while CO chemisorbs on these metals with considerable electron transfer from the metals to its $2\pi^*$ antibonding orbital. Such strong metal-mediated interactions obscure the subtle effects usually associated with supramolecular structures.

* To whom correspondence should be addressed. E-mail: hipps@wsu.edu.

10.1021/jp026875c CCC: $25.00
Published on Web 03/08/2003

While it may never be possible to totally eliminate adsorbate−substrate interactions (see the discussion concerning surface dipole moments), significantly reducing them is possible. An example of weak intermolecular interactions combined with physisorption comes from the STM study of DNA base molecules on Cu(111).[23] DNA base molecules form novel superstructures on Cu(111) surfaces through intermolecular hydrogen bonding and through their planar orientation on the surface. STM images revealed that the relative inertness of the Cu(111) substrate allows the molecules to diffuse over the surface to spontaneously self-assemble themselves into small clusters and chains. Because of this rapid diffusion, single isolated molecules cannot be seen at room temperature. Of the bases studied, adenine gives the clearest evidence of hydrogen bonding controlled structure, producing one-molecule-wide chains on Cu(111). Very recently, Yokoyama and co-workers have observed similar small clusters and chains on Au(111) at 63 K.[24] In this study, cyanophenyl-substituted porphyrins were found to form three-molecule clusters for single substitution, four-molecule clusters for asymmetric double substitution, and branching chains for symmetrical double substitution.

While these reports on DNA bases and cyanophenyl-substituted porphyrins are encouraging for one-dimensional (1D) aggregation, they do not represent practical examples of 2D supramolecular structures because (1) there is not one highly preferred structure that can be grown with finite extent in the surface plane, (2) it is not clear that the structures seen to date on Au(111) are entirely the result of rational design since there appears to be a preference for ordering induced by the Au(111) reconstruction, and (3) the really well-ordered structures have only been observed at very low temperature. Even in the case of 1D structures (chains) the extent to which the reported structures resulted from rational design is in question because unsubstituted phthalocyanines also form chains on Au(111) at low temperature.[25,26]

Below 100 K, 1-nitronaphthalene adsorbed on Au(111) aggregates into distinct structures whose dimensionality depend on the coverage.[27] At 1-nitronaphthalene coverage around 0.05 ML, trimers nucleate at the elbows of the herringbone reconstruction. At coverage between 0.05 and 0.15 ML decamers are observed. At medium coverage (0.3−0.75 ML), the growth mode changes to the formation of 1D molecular double chains. The double chains are guided by the reconstruction domains or by step edges. Finally, at full monolayer coverage 1D and 2D periodic molecular structures coexist on the surface. H-bonding between O and a proton on an adjacent ring is thought to drive the long range structure. These structures only exist at low temperature because of the very weak substrate−adsorbate interactions.

Barth et al.[28] have provided an excellent example of a 1D-ordered supramolecular structure. Adsorption of 4-[*trans*-2-(pyrid-4-yl-vinyl)]benzoic acid (PVDA) was studied by variable temperature STM. The subject molecule was vapor deposited under UHV conditions onto Pd(110), Cu(111), and Ag(111), with the strength of adsorption decreasing in the order Pd > Cu > Ag. On Pd(110), only isolated molecules are seen. On Cu(111) both filaments and isolated molecules are observed. On Ag(111) complex aggregation of flat laying molecules is seen for 125K adsorption. Adsorption at 300 K (but measured at 77 K) on Ag(111) results in long chains consisting of pairs of PVDA, with each pair chain separated by about 5 nm from others. This clearly emphasizes our point that because molecular self-assembly at surfaces is governed by the balance between intermolecular and molecule−surface interactions, relatively weak adsorbate−substrate interactions are required to allow rational 2D design on the basis of weak intermolecular forces.

There are reports of highly ordered 2D structures at the solution−graphite interface where solvent and solute adopt well-defined bimolecular structures.[29,30] The first example of two different solutes and a solvent forming a well-ordered 2D structure on graphite was provided by Flynn's group.[31,32] While these reports offer insights into supramolecular aggregation and provide potential pathways to new 2D materials, the role of the solvent in the structure and the kinetics of adsorption and desorption are probably playing a significant role in determining the observed structures. For example, Beebe has shown that the typical residence time of a solute molecule in a graphite-supported monolayer appears to be between 0.2 and 20 s.[33] Solution phase adsorption of covalently bound systems on gold have also yielded 2D-ordered structures.[34] These systems, however clearly cannot be described as having weak adsorbate−surface interactions. To our knowledge, the only report of a well-ordered single-component 2D structure resulting from directed weak intermolecular forces and physisorption from the vapor (onto graphite) was provided by Griessl et al.[35] Adsorption of trimesic acid on single-crystal graphite was studied under UHV conditions. Two coexisting phases could be imaged with submolecular resolution by STM. Induced by directed hydrogen bonding, the organic molecularly built 2D-grid architecture with molecular caves. Both a "chicken wire" structure and a "flower" structure were observed.

In a recent communication we provide the first example of a bimolecular self-assembled 2D structure formed by vapor phase deposition onto a metal surface.[36] That system is discussed here in much greater detail. It is a two component structure reminiscent of the fluorophenyl−phenyl system, but modified to reflect the 2D nature of the problem. Conceptually, we thought of the fluorine−hydrogen bonding as the supramolecular interaction, the synthon, that drove the ordering process. As we will discuss, the overall picture is more complex. In any case, the coadsorption of porphyrin and fluorinated phthalocyanine results in a new bimolecular structure that is demonstrated by scanning tunneling microscopy (STM) under UHV conditions at room temperature. In addition, RAIRS, UPS, and XPS spectroscopic results will be used to characterize the individual compounds as thin films.

Experimental Section

The materials studied in this report include cobalt(II) 1,2,3,4,8,9,10,11,15,16,17,18,22,23,24,26-hexadecafluoro-29*H*,31*H*-phthalocyanine, $C_{32}CoF_{16}N_8$ [F16CoPc], and nickel(II) 5,10,15,20-tetraphenyl-21*H*,23*H*-porphine, $C_{44}H_{28}N_4Ni$ [NiTPP], as shown in Figure 1, and the fully protonated form of cobalt(II) phthalocyanine, CoPc. These compounds were obtained from Aldrich and were purified by sublimation. The gold metal used was either 99.999% gold splatters (for deposition), or 99.985% gold foil (for XPS and UPS studies).

Vapor deposition of organic compounds was performed either from quartz crucibles or tantalum boats. The temperature of the sources was monitored with iron−constantan thermocouples, with the temperature of the F_{16}CoPc being the critical parameter. At temperatures above about 450 °C, a 200 amu signal increased dramatically suggesting decomposition of the organic compound.[37] A quartz thin-film monitor was used to measure the deposition rate for each component. Density values of 1.4, 2.4, and 1.6 g/cm^3 were used for NiTPP, F16CoPc, and CoPc, respectively. The residual gases during deposition were monitored with a quadrupole mass spectrometer to demonstrate that no low-mass fragments were created by thermal decomposition.

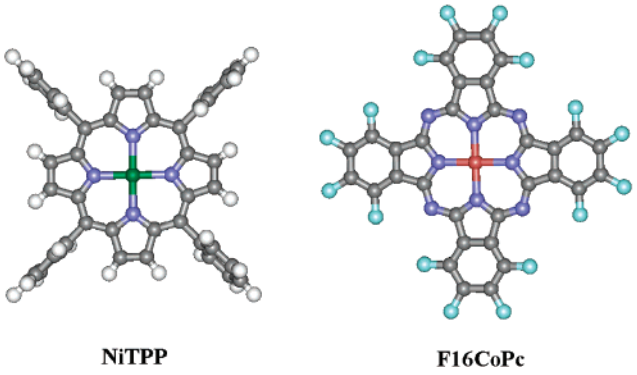

Figure 1. Structures of F_{16}CoPc and NiTPP. The color code used is as follows: carbon is gray, hydrogen is white, nitrogen is dark blue, fluorine is light blue, cobalt is red, and nickel is green.

IR Spectroscopy. Samples for reflection−absorption infrared spectroscopy (RAIRS)[38] were prepared as follows: 200 nm of Al was first deposited onto precleaned glass microscope slides and then 30 nm of Au was deposited on the Al film. Three such substrates were made at one time. Organic films of different thicknesses were deposited on two of the substrates. The third was used as a reference. The gold was deposited at a rate of 0.17 nm/s while the organic compound was deposited at 0.07 nm/s. Alternatively, <1 mg of the pure compound was thoroughly ground with 100 mg of KBr and pressed into a pellet. A pure KBr pellet was used as a reference. These KBr-based samples were measured in transmission mode in the same IFS 113 spectrometer. For the IR measurements, a globar source, Ge-coated KBr beam splitter, and a wide band LN2 cooled HgCdTe detector were used. The bench pressure was maintained below 20 mTorr throughout the measurement cycle. RAIRS spectra were acquired at an angle of incident of 86° and 8 cm^{-1} resolution. Typical RAIRS spectra are the result of 8000 scans. Transmission IR spectra were obtained with 4 cm^{-1} resolution and 256 scans averaged.

XPS and UPS Spectroscopy. Gold foil was used as a substrate and cleaned by heating and argon ion etching before use. The organic compounds were thermally deposited onto the gold foil in a UHV prep-chamber attached to the spectrometer. The thickness of the film was determined with a quartz crystal microbalance. In addition, XPS spectra of the original powders pressed into indium foil (99.99%) were also measured.

A Kratos Axis 165 multitechnique electron spectrometer was used to acquire both XPS and UPS spectra. 280 W of achromatic X-radiation at energy 1253.6 eV (MgKα) was used as XPS excitation source. The analyzer was set for a spatial resolution of 120 μm. The energy resolution was set to 1.3 eV for survey spectra and 0.75 eV for the high-resolution acquisitions of C 1s, N 1s, M 2p, and Au $4f_{7/2}$ peaks. Binding energies were calibrated against the Au $4f_{7/2}$ peak taken to be located at BE = 84 eV. UPS spectra were excited using a homemade helium lamp and an electrostatic lens focused the ejected electrons into the spectrometer. All data reported were acquired with the He I line at 21.22 eV. A bias of −10 V was applied to the samples to shift the spectra out of the nonlinear region of the analyzer (KE = 0−10 eV). The spectrometer was used in fixed analyzer transmission mode (FAT) with pass energy of 20 eV and spatial resolution of 120 μm. The resolution of our homemade UPS system is about 150 meV as determined at the Fermi edge of a single crystal of gold.

STM Sample Preparation and Data Acquisition: Epitaxial Au(111) films with well-defined terraces and single atomic steps were prepared on mica by previously described methods.[39−43]

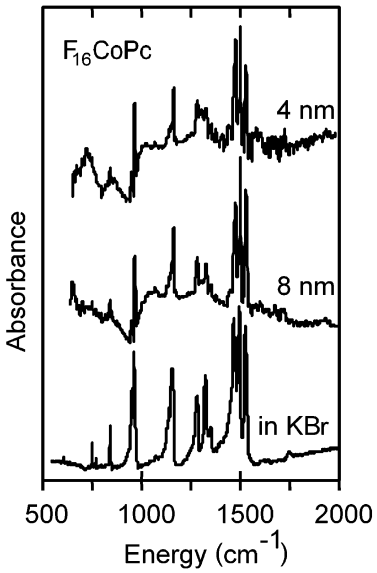

Figure 2. Infrared spectra of F_{16}CoPc. The spectrum of the authentic powder pressed in KBr is compared to those of 4 and 8 nm thick vapor-deposited films on polycrystalline gold.

These films were 0.1−0.2 μm thick and had a mean single-grain diameter of about 0.3 μm. Unlike true single-crystal gold,[44] these small crystal grains showed reconstruction line spacing ranging from 6.3 to about 9.0 nm. The gold films were transferred via air-lock into the UHV STM chamber (working pressure ~2×10^{-10} Torr) where the compounds were deposited and then studied without exposure to air. In some cases, the compounds were deposited in a second chamber and transferred through air to the STM chamber. The STM head used was produced by McAllister Technical Services (Coeur d'Alene, ID) and is of the inertial approach type. A Digital Instruments Nanoscope III controller was used to acquire the reported data. STM image analysis was performed with the SPIP commercial software package. Constant current images are reported and any filtering is indicated in the appropriate figure caption. All images were acquired at about 21 °C. Both etched W and cut $Pt_{0.8}Ir_{0.2}$ tips were used. Generally, the W tips required a UHV cleaning step (electron beam bombardment) in order to produce high-quality images.

Results and Discussion

We have previously reported the IR and XPS spectra of thin films of CoTPP and NiTPP.[42,43] The KBr pellet IR and RAIRS of F_{16}CoPc vapor deposited on Au are shown in Figure 2. These three spectra are very similar in terms of peak positions and differ only slightly in relative band intensities. We interpret this to mean that these relatively thick (≥4 nm) films are not uniformly oriented with the ring parallel to the gold surface. Since most of the intense bands in this region of the spectrum are due to in plane stretches, their appearance in the RAIRS is clear evidence that the high-symmetry (4-fold) axis must, on the average, make an angle smaller than 90° with respect to the surface. This result is also consistent with a disordered film (vide infra) on gold. The important conclusion here is that vapor deposition under the stated conditions can be used to form films with the same chemical structure as that of the starting material.

XPS spectra of CoPc and F_{16}CoPc were recorded both for thin films and powders and some of the observed peak positions are reported in Table 1. Also presented in Table 1 are the reported XPS peak positions observed for F_{16}CuPc adsorbed on Si(100)[45] and on Si(111).[46] The values given in the table for

TABLE 1: XPS Peaks for F_{16}CoPc and Comparison to Similar Compounds

element	BE (eV)[a] F_{16}CoPc/Au 0.5 nm film	BE (eV)[a] F_{16}CoPc powder	BE (eV)[b] F_{16}CuPc	BE (eV)[a] CoPc/Au 1.0 nm film	intensity ratio observed for F_{16}CoPc/Au	intensity ratio theoretical
C 1s	284.8	284.6	285.0	284.7	C/F = 2.1	C/F = 2.0
	286.9	286.4	287.2			
N 1s	398.9	398.6		398.5	C/N = 3.8	C/N = 4.0
F 1s	687.3	687.2	687.3		F/N = 2.2	F/N = 2.0
Co(II) $2p_{3/2}$	780.9	780.7		780.6	Co/N = 0.13	Co/N = 0.125

[a] This work. [b] Binding energy from refs 45 and 46.

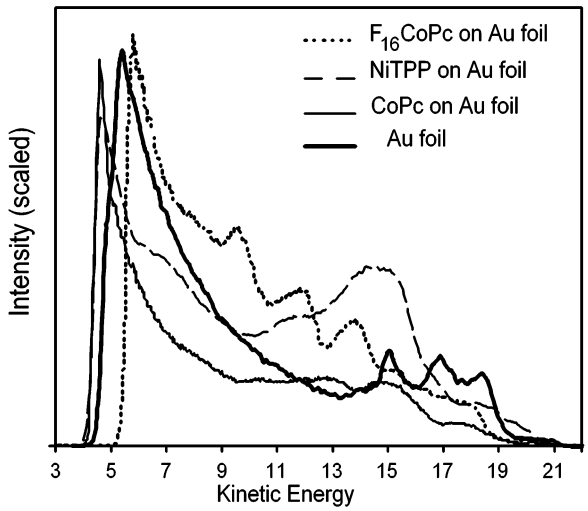

Figure 3. Wide-range UPS spectra of less than 2 nm thick films of CoPc, F_{16}CoPc, NiTPP, supported on gold foil, and of the clean gold foil substrate. Note that the low kinetic energy cutoff for NiTPP and CoPc occurs at the same energy, but somewhat lower kinetic energy than the gold foil. The low-energy cutoff of F_{16}CoPc, on the other hand, occurs at higher kinetic energy than does the cutoff of gold foil.

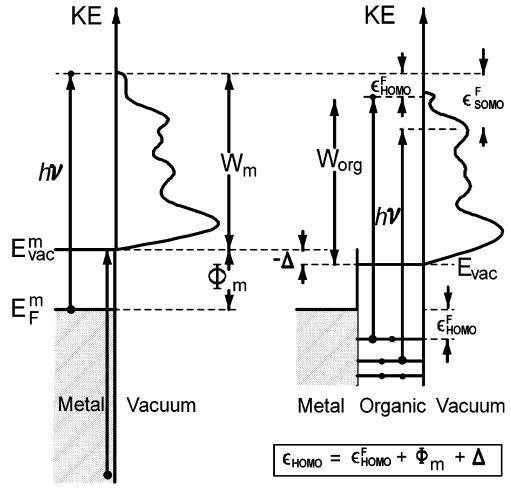

Figure 4. Schematic representation of energy levels involved in the photoelectron spectrum of a clean metal (left) and of the same metal coated with a thin organic layer. The energy of the vacuum level over the organic relative to that of the clean metal is given by the quantity Δ (shown for the case where Δ is negative). The work function of the metal is given by Φ_m, and can be calculated from the relationship $h\nu = W_m + \Phi_m$, where W_m is the width of the photoelectron spectrum in eV. Also note that the energy of the occupied orbitals relative to the vacuum level is given by $\epsilon^F + \Phi_m + \Delta$.

CoPc are also in good agreement with those reported by Paez-Mozo et al.[47] It is worth noting the significant splitting of the C 1s peak. The lower binding energy peak near 284.8 eV is very similar to the (only) peak observed in the nonfluorinated compound. The higher energy peak near 287 eV clearly originates from the carbons directly bonded to fluorine. This large increase in binding energy reflects the withdrawal of valence electrons from carbon by fluorine. Because a monolayer of F_{16}CoPc is of the order of 0.4 nm thick, and since the XPS peak positions for the 0.5 nm film on Au agree well with those of the powder, we can confidently assert that F_{16}CoPc adsorbs without decomposition on the gold surface.

Figure 3 displays wide range He I UPS spectra of CoPc, F_{16}CoPc, and NiTPP vapor deposited on gold foil. All organic films are less than 2 nm thick. Also shown in Figure 3 is a typical He I UPS spectrum of clean gold foil substrate. Note that the low kinetic energy cutoff for NiTPP and CoPc occurs at the same energy, but 0.40 eV lower kinetic energy than the gold foil. The low-energy cutoff of F_{16}CoPc, on the other hand, occurs 0.8 eV higher in kinetic energy than does the cutoff of gold foil. These shifts in apparent vacuum level are depicted schematically in Figure 4. The energy of the vacuum level over the organic relative to that of the clean metal is given by the quantity Δ (shown for the case where Δ is negative). The work function of the metal is given by Φ_m, and can be calculated from the relationship $h\nu = W_m + \Phi_m$, where W_m is the width of the photoelectron spectrum in eV. We found that $\Phi_m = 4.70 \pm 0.15$ eV for the gold foil used in these experiments. Also note that the energy of the occupied orbitals relative to the vacuum level is given by

$$\epsilon = \epsilon^F + \Phi_m + \Delta \quad (1)$$

where ϵ is the energy of an occupied state relative to the vacuum level and ϵ^F is the energy relative to the Fermi level of the metal contact.

The CoPc and NiTPP cases are as depicted in Figure 4 and $\Delta = -0.40$ eV. This reflects the somewhat positive charge developed by the organic layer relative to the gold surface and is consistent with the fact that these are p-type semiconductors. F_{16}CoPc, on the other hand, is an n-type semiconductor, as would be expected due to the strong electron withdrawing power of the fluorines. Thus, it is not too surprising that the F_{16}CoPc film has $\Delta = +0.8$ eV and is polarized negatively with respect to the gold surface. For later reference, note that the negative polarization on the fluorinated compounds is about 2 times greater in magnitude than that of either NiTPP or of CoPc.

Figure 5 presents the He I UPS low binding energy region of the spectra obtained from < 2 nm thick films of CoPc and F_{16}CoPc on gold foil. In Figure 5, the energy of the Fermi level of the gold foil is taken as zero. Making use of eq 1, we find that the HOMO energy for CoPc is $1.05 + 4.70 - 0.40 = 5.35$ eV, while that for F_{16}CoPc is $1.50 + 4.70 + 0.8 = 7.0$ eV. We note that these values are in good agreement with those reported (5.35 and 6.88, respectively) by Schlettwein et al.[48] We also note here that the shifts Δ were measured relative to the foil substrate before and after the compound deposition and varied

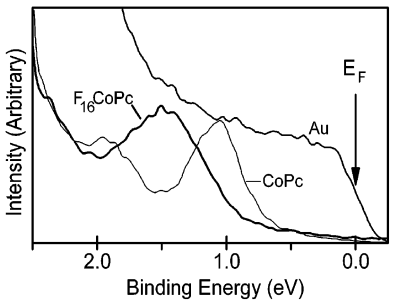

Figure 5. He I UPS binding energy (relative to the Fermi energy) plot for CoPc and F_{16}CoPc near the Fermi energy of the gold foil substrate. The organic films were thermally deposited on gold foil and were less than 2 nm thick.

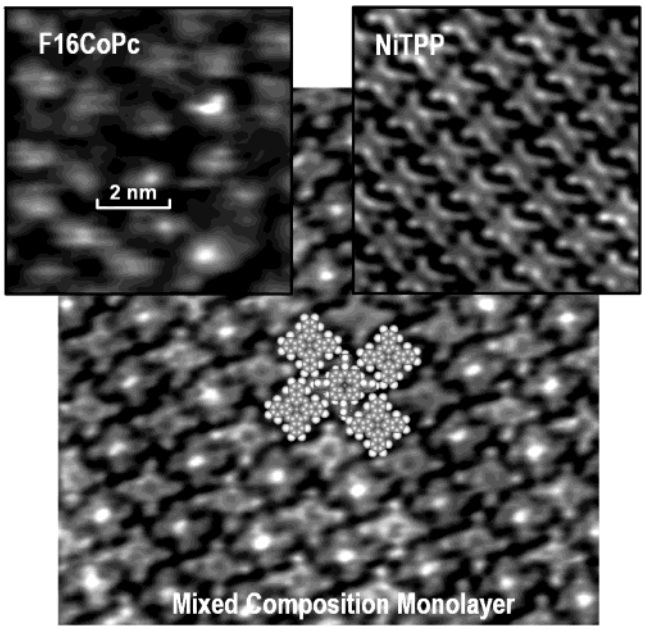

Figure 6. Comparison of room-temperature constant current STM images of different organometallics adsorbed on Au(111) imaged under UHV conditions. In the upper right is a high-resolution image of NiTPP was acquired at −1.0 V sample bias and 0.4 nA. In the upper left is a high-resolution image of F_{16}CoPc acquired at 0.9 V sample bias and 0.15 nA. The deposition rate for both compounds was 0.01 nm/s for a total exposure of about 0.2 nm. The lower center image was obtained from a 2:1 molar ratio deposition of NiTPP and F_{16}CoPc on Au(111). A constant current of 0.35 nA and a sample bias of +0.4 V was used. The high-resolution NiTPP and mixture images were Fourier filtered. The scale bar applies to all parts of this figure.

somewhat (±0.15 eV) from deposition to deposition. Thus, Δ cannot be determined for all three compounds from the data in Figure 3.

Constant current STM images of near monolayer coverage films obtained under UHV conditions at room temperature are shown in Figure 6. The top right image shows a high-resolution image of NiTPP adsorbed on Au(111). The phenyl rings of the TPP ligand are oriented nearly perpendicular to the gold surface. NiTPP molecules form a well-ordered close-packed 2D structure. This structure and its electronic properties have been discussed in some detail, previously.[42,43] Isolated NiTPP molecules are never observed on atomically flat terraces (single molecules are sometimes seen at the step edges) at room temperature due to surface diffusion, demonstrating the weak interaction between adsorbate and substrate that we require for our model system. The NiTPP molecules in this insert do not appear to have 4-fold symmetry. Images taken on several samples with several tips vary in that some appear to have 4-fold symmetry while others do not. While we have attributed this to asymmetries in the tip and thermal drift, it may be that we are occasionally observing deformation in the porphyrin ring similar to that observed by Yokoyama at al.[49]

A high-resolution STM image of F_{16}CoPc adsorbed on Au(111) is shown in the top left image of Figure 6. Although these molecules tend to aggregate, they do not form an ordered structure when deposited on Au(111). Further, there is considerable thermal motion on the surface causing the high-resolution images to appear with no submolecular resolution. The disorder and lack of submolecular resolution for F_{16}CoPc is in dramatic contrast to what occurs for the protonated complex, CoPc. Films of CoPc form large 2D crystalline islands and individual molecules can be imaged with exquisite submolecular resolution.[39,40] Why do low-coverage films of CoPc order while similar F_{16}CoPc films do not? This significant difference in packing between the proto and fluoro phthalocyanine can probably be traced to differences in van der Waals attraction and electron affinities. In the free molecular form, the fluorinated compound, is strongly negatively charged at its periphery while the unfluorinated CoPc is much less intensely positively charged. In addition to the direct repulsion between negatively charged fluorines, one must also consider the through-metal interactions and the differences in adsorption energy that result from the differences in electronic state energies. All of these effects are reflected in the surface film properties as demonstrated by the vacuum level shift of F_{16}CoPc on Au, $\Delta = +0.8$ V, relative to that of CoPc adsorbed on Au, $\Delta = -0.4$ V.

The main image was obtained from a film that results when NiTPP and F_{16}CoPc are deposited in a 2:1 molar ratio onto Au(111) at room temperature. This sample was prepared by alternately exposing the substrate for 1 and 2 s to F_{16}CoPc and NiTPP vapor, respectively. The sample was grown with a total exposure time of 21 s at a deposition rate of about 0.01 nm/s. In the main image of Figure 6, the F_{16}CoPc molecules are easily distinguished from the NiTPP molecules by the strong tunneling current that results from orbital-mediated tunneling through the half-filled d_{z^2} orbital of the Co^{2+} ion—they appear to have high spots in the center. The NiTPP molecules show a depression in the center consistent with the filled d_{z^2} orbital of the Ni^{2+} ion. We also note that NiTPP in this mixed composition structure always appears to have 4-fold symmetry. The remarkable contrast in tunneling current afforded by the difference in electronic configurations of transition metal ions allows one to clearly label molecular species for chemical identification at the molecular level.[39,40,42] Unlike the films that result when F_{16}CoPc alone is deposited on Au(111), the mixture has ordered regions where the individual F_{16}CoPc molecules are clearly seen with submolecular resolution. Even the orientation of the phenyl groups in NiTPP is easily observed. Moreover, the area shown in Figure 6 is clearly a well-ordered 1:1 structure with each F_{16}CoPc surrounded by four NiTPP molecules. Clearly, the *intermolecular interactions between F_{16}CoPc and NiTPP are producing an entirely new 2D crystalline structure that is more stable than the films resulting from either parent compound.*

A critical question here is, How far does this order extend? Figure 7 depicts a typical wide area image obtained from the same film as shown in the central part of Figure 6. Figure 7 demonstrates that under the deposition conditions used, three types of regions result: disordered regions containing both F_{16}CoPc and NiTPP (region C), well-ordered domains of NiTPP (as in B), and well-ordered regions of the new 1:1 composition structure, A. The nature of each of these is verified by high-resolution imaging. The parallel striations seen in this figure

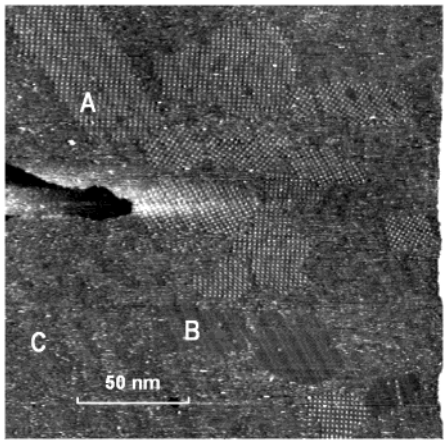

Figure 7. A wide-area low-resolution image of a 2:1 molar ratio deposition of NiTPP and F_{16}CoPc on Au(111). A constant current of 0.35 nA and a sample bias of −0.6V was used.

are due to the underlying Au(111) reconstruction. Figure 7 shows islands of this new 1:1 material that are ∼100 nm in extent. Analysis of many such images taken from several samples indicates that these ordered regions represent about 25% of the surface. Preliminary experiments indicate that it should be possible to grow these islands much larger, perhaps to entirely cover a metal support. Parameters that produce changes in island size are (1) deposition rate, (2) relative rates of arrival of the components, (3) substrate temperature during deposition, and (4) postdeposition annealing. Modifications of these layers in terms of both electron transport properties and the addition of vertical substituents through changes in the central metal ion are easily engineered. We believe this is only the first in a broad new class of materials that can result as a consequence of both weak intermolecular interactions and image charges associated with adsorption on metal surfaces. What remains to be seen is whether these structures can be extended upward by sequential deposition to produce new three-dimensional materials.

As seen in Figure 8, similar films made from the all protoforms of CoPc and NiTPP are densely packed and appear to have a well-defined structure, but are compositionally disordered. This type of disorder can be found in the literature.[40] While both films were deposited with a 2:1 ratio of tetraphenylporphyrin to phthalocyanine, of the area shown of the nonfluorinated material has a measured ratio of 7:5. The NiTPP/CoF_{16}Pc film has a 1:1 composition ratio. The fluorine substitution is clearly driving the formation of the well-ordered and stoichiometric structure.

Conclusions

While the remarkable ordering seen in the 1:1 compound layer is clearly due to interactions resulting from the presence of protonated and fluorinated species, more work is required to identify the principle driving forces for the ordering. This is because in the adsorbed state on a conductive surface, the fluorine−hydrogen intermolecular interactions are not necessarily the only important synthons. One can enumerate some of the interactions, which may drive this ordering. These include the ability of the two types of molecules to interlace, the up to 4kJ/mol attractive energy for each close-approach H···F interaction,[50] and reduced electrostatic repulsion between F_{16}CoPc molecules due to the increased spacing forced by the NiTPP units. The attraction between the dipole moments normal to the surface at the periphery of each molecule that result from image charge formation in the substrate must also be considered. An

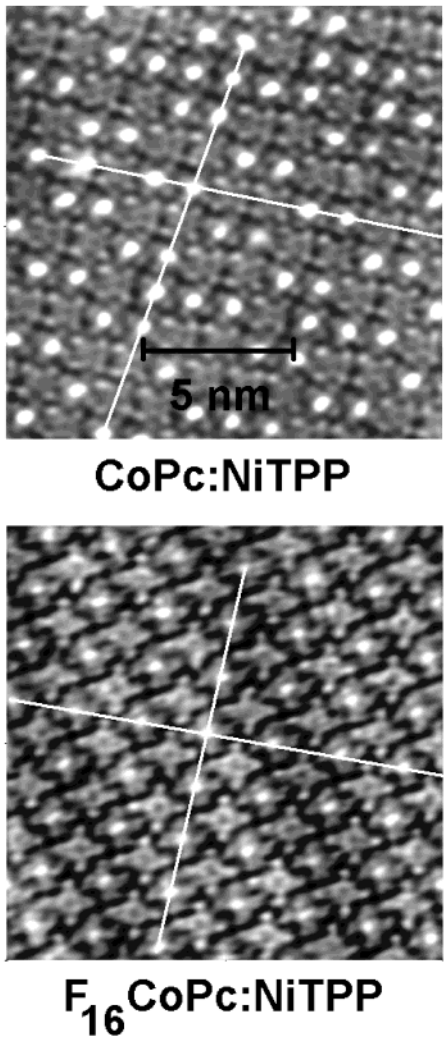

Figure 8. High-resolution images of a 2:1 molar ratio deposition of NiTPP with CoPc (top), and with F_{16}CoPc (bottom) on Au(111). Deposition and measurement conditions were identical. The scale bar applies to both parts of the figure.

additional metal-mediated interaction can occur via shifts in electronic states associated with differing admixtures of metal surface states. Finally, there is the destabilizing but weak quadrupole repulsion between the vertically oriented phenyl groups and the horizontally oriented fluorinated Pc ring.

In the introduction of this paper we mentioned the CO/benzene system and said it was not an example of weak intermolecular forces driving order. The primary driving force in that case was identified as charge transfer (with the metal) induced dipole−dipole interactions. It turned out, however, that such dipole−dipole interactions also occur in the molecular systems studied here. While we believe they play a minor role in determining the ordered structure observed in this report, they certainly help stabilize it. In fact, it is hard to image an H bonding system where there will be no participation from dipoles induced normal to the metal surface. Thus, the surface−normal dipole interactions will almost always play some role in determining the surface structure of adsorbates. We are led again to our original contention that the combination of weak intermolecular interactions (like hydrogen bonding) combined with the template effect of the surface and the image charge interactions produced by the metal substrate make a particularly appropriate set of building blocks for new and exciting supramolecular structures.

Acknowledgment. Acknowledgment is made to the donors of the Petroleum Research Fund, administered by the ACS, and to the National Science Foundation for its support in the form of Grant 0138409. William A. English assisted with UPS studies.

References and Notes

(1) Lehn, J. N. *Supramolecular Chemistry: Concepts and Perspectives*; VCH: Weinheim, Germany, 1995.
(2) Atwood, J. L., Davies, J. E., Macnicol, D. D., Vogtle, F., Eds. *Comprehensive Supramolecular Chemistry*; Pergamon Press: New York, 1996.
(3) Desiraju, G. R. *Angew. Chem., Int. Ed. Engl.* **1995**, *34*, 2311.
(4) Scmhidt, G. M. *Pure Appl. Chem.* **1971**, *27*, 647.
(5) Reddy, D. S.; Ovchinnikov, Y.; Shishkin, Y.; Struchkov, Y.; Desiraju, G. *J. Am. Chem. Soc.* **1996**, *118*, 4085 and references therein.
(6) Xu, K.; Ho, D.; Pascal, R. *J. Org. Chem.* **1995**, *60*, 7186.
(7) Coates, G.; Dunn, A.; Henling, A.; Dougherty, D.; Grubbs, R. H. *Angew. Chem., Int. Ed. Engl.* **1997**, *36*, 248.
(8) Coates, G.; Dunn, A.; Henling, L.; Ziller, J.; Lobkovsky, E.; Grubbs, R. H. *J. Am. Chem. Soc.* **1998**, *120*, 3641.
(9) Gillard, R.; Stoddard, J.; White, A.; Williams, B.; Williams, D. *J. Org. Chem.* **1996**, *61*, 1**,** 4504.
(10) Williams, J. H. *Acc. Chem. Res.* **1993**, *26*, 593.
(11) Hunter, C.; Lu, X.; Kapteijn, G.; Koten, G. *J. Chem. Soc., Faraday Trans.* **1995,** *91*, 2009.
(12) Bosch, E.; Radford, R.; Barnes, C. *Org. Lett.* **2001**, *3*, 881.
(13) Marsella, M. J.; Wang, Z.; Reid, R.; Yoon, K. *Org. Lett.* **2001**, *3*, 885.
(14) West, A.; Mecozzi, S.; Dougherty, D. *J. Phys. Org. Chem* **1997**, *10*, 347.
(15) Alkorta, I.; Rozas, L.; Elguero, J. *J. Org. Chem.* **1997**, *62*, 4687.
(16) Hernandez-Trujillo, J.; Colmenares, F.; Cuevas, G.; Costas, M. *Chem. Phys. Lett.* **1997,** *265*, 503.
(17) Ohtani, H.; Bent, B.; Mate, C.; Van Hove, M.; Somorjai, G. A. *Appl. Surf. Sci.* **1988**, *33/34*, 254.
(18) Ohtani, H.; Wilson, R.; Chiang, S.; Mate, C. M. *Phys. Rev. Lett.* **1988**, *60*, 2398.
(19) Hallmark, V. M.; Chiang, S. *Surf. Sci.* **1995**, *329*, 255.
(20) Yoon, H.; Salmeron, M.; Somorjai, G. A. *Surf. Sci.* **1997**, *373*, 300.
(21) Mate, C. M.; Kao, C.; Somorjai, G. A. *Surf. Sci.* **1988**, *206*, 145.
(22) Salmeron, M.; Dunphy, J. *Faraday Discuss.* **1997**, *105*, 151.
(23) Kawai, T.; Tanaka, H.; Nakagawa, T. *Surf. Sci.* 1997, *386*, 124.
(24) Yokoyama, T.; Yokoyama, S.; Kamikado, T.; Okuno, Y.; Mashiko, S. *Nature* **2001**, *413*, 619.
(25) Barlow, D.; Scudiero, L.; Hipps, K. W. In preparation.
(26) Walzer, K.; Hietschold, M.; *Surf. Sci.* **2001**, *471*, 1.
(27) Schneider, W. D. *Phys. Status Solidi A* **2001**, *187*, 125−136.
(28) Barth, J.; Weckesser, J.; Cai, C.; Günter, P.; Bürgi, L.; Jeandupeux, O.; Kern, K. *Angew. Chem., Int. Ed.* **2000**, *39*, 1230.
(29) De Feyter, S.; Grim, P. C.; Rucker, M.; Vanoppen, P.; Meiners, C.; Sieffert, M.; Valiyaveettil, S.; Mullen, K.; Schryver, F. C. *Angew. Chem., Int. Ed.* **1998,** *37*, 1223.
(30) De Feyter, S.; Gesquière, A.; Grim, P.; De Schryver, F.; Valiyaveettil, S.; Meiners, C.; Sieffert, M.; Mullen, K. *Langmuir* **1999**, *15*, 2817.
(31) Yablon, D.; Giancarlo, L.; Flynn, G. W. *J. Phys. Chem. B* **2000,** *104*, 7627.
(32) Yablon, D.; Guo, J.; Knapp, D.; Fang, H.; Flynn, G. W. *J. Phys. Chem. B* **2001,** *105*, 4313.
(33) Stevens, F.; Beebe, T. P. *Langmuir* **1999**, *15*, 6884.
(34) Pinheiro, L. S.; Temperini, M. L. *Surf. Sci.* **1999**, *441*, 45.
(35) Griessl, S.; Lackinger, M.; Edelwirth, M.; Hietschold, M.; Heckl, W. *Single Mol.* 2002, *1*, 25.
(36) Hipps, K. W.; Scudiero, L.; Barlow, D.; Cooke, M. *J. Am. Chem. Soc.* **2002**, *124*, 2126.
(37) Schlettwein, D.; Hesse, K.; Tada, H.; Mashiko, S.; Storm, U.; Binder, J. *Chem. Mater.* **2000**, *12*, 989.
(38) Greenler, R. G.; Rahn, R. R.; Schwartz, J. P. *J. Catal.* **1971**, *23*, 42.
(39) Lu, X.; Hipps, K. W. *J. Phys. Chem. B* **1997**, *101*, 5391.
(40) Lu, X.; Hipps, K. W.; Wang, X.; Mazur, U. *J. Am. Chem. Soc.* **1996**, *118*, 7197.
(41) Barlow, D.; Hipps, K. W. *J. Phys. Chem. B* **2000**, *104*, 2444.
(42) Scudiero, L.; Barlow, D.; Hipps, K. W. *J. Phys. Chem. B* **2000**, *104*, 11899.
(43) Scudiero, L.; Barlow, D. E.; Mazur, U.; Hipps, K. W. *J. Am. Chem. Soc.* **2001**, *123*, 4073.
(44) Barth, J. V.; Brune, H.; Ertl, G.; Behm, R. J. *Phys. Rev. B* **1990**, *42*, 9307.
(45) Lozzi, L.Ottaviano, L.; Santucci, S. *Surf. Sci.* **2001**, *507*−*510*, 351.
(46) Lozzi, L.; Santucci, S. *Surf. Sci.* **2001**, *482*−*485*, 669.
(47) Paez-Mozo, E.; Gabriunas, N.; Lucaccioni, F.; Acosta, D.; Patrono, P.;La Ginestra, A.; Ruiz, P.; Delmon, B. *J. Phys. Chem.* **1993**, *97*, 12819.
(48) Schlettwein, D.; Hesse, K.; Gruhn, N.; Lee, P.; Nebesny, K.; Armstrong, N. R. *J. Phys. Chem. B* **2001,** *105*, 4791.
(49) Yokoyama, S.; Kamikado, T.; Mashiko, S. *J. Chem. Phys.* **2001**, *115*, 3814−18.
(50) DerHovanessian, A.; Doyon, J. B.; Jain, A.; Rablen, P.; Sapse, A. *Org. Lett.* **1999**, *1*, 1359.